Conformational interconversions in supersonic jets: Matrix IR spectroscopy and model calculations

ARTICLE *in* CHEMICAL PHYSICS · SEPTEMBER 1982

Impact Factor: 1.65 · DOI: 10.1016/0301-0104(82)87002-X

2 AUTHORS, INCLUDING:

Peter Felder
University of Zurich
51 PUBLICATIONS **1,255** CITATIONS

Chemical Physics 71 (1982) 9–25
North-Holland Publishing Company

CONFORMATIONAL INTERCONVERSIONS IN SUPERSONIC JETS: MATRIX IR SPECTROSCOPY AND MODEL CALCULATIONS

Peter FELDER* and Hs.H. GÜNTHARD ‡
Laboratory for Physical Chemistry, Swiss Federal Institute of Technology, ETH Zentrum, CH-8092 Zurich, Switzerland

Received 2 March 1982

Terminal conformer populations in supersonic molecular beams have been measured by use of matrix IR spectroscopy. The experimental technique is based on trapping of the beam molecules into a cryogenic matrix. The ratio of conformational isomers is determined by comparing intensity ratios of infrared absorption bands with those found in analogous experiments with thermal effusive molecular beams. For supersonic beams of pure 1,2-difluoroethane a considerable depopulation of the less stable trans conformer is found, the lowest terminal conformational temperature reached being $T_c^{\infty} = 207(3)$ K. In seeded argon beams the cooling of the conformational distribution was found to be weaker. In supersonic beams of 1,2-dichloroethane and of methyl nitrite no significant conformational cooling was found. The experimental results are discussed in terms of a kinetic model of conformational interconversion in the flow field of a continuum free jet. The calculations indicate that conformational cooling by supersonic expansion may be expected only for molecules with a low energy barrier to internal rotation.

1. Introduction

The application of molecular-beam methods to a variety of problems in chemical physics has been growing steadily in the last 15 years. One of the reasons for this growth was the advent of the supersonic-beam technique, in which the molecular beam is formed by sampling a free jet emerging from a convergent nozzle. For a review the reader is referred to Anderson [1] and to Levy et al. [2].

In addition to the obtainable high intensity, the supersonic-nozzle method offers the advantage of a narrow velocity spread of the beam molecules. This fact is due to the near-adiabatic cooling taking place in the free-jet expansion. Owing to the highly non-uniform character of the expansion zone, the dynamics of relaxation processes occurring in it are difficult to describe. Much effort has been spent to study the energy transfer between the translational, rotational and vibrational molecular degrees of freedom in such expansions.

It is now quite well established that molecules in supersonic beams experience strong translational and rotational cooling. For vibrational degrees of freedom the situation is less clear, vibrational relaxation efficiencies having been found to cover a rather large range. As a rule, however, vibrational cooling is considerably weaker than rotational cooling. A review of work done in this area has been given by McClelland et al. [3].

It should perhaps be mentioned that in the context of free-jet expansions the word "cooling" is used to describe processes in which populations of energy levels are shifted to states of lower energy, but without requiring the existence of a thermodynamic temperature.

In this publication we report investigations using supersonic beams of molecules with two conformational isomers. One of the goals was to ascertain under which conditions a free-jet expansion has a cooling effect on conformer populations.

In a previous study with supersonic jets of pure 1,2-difluoroethane and of methyl nitrite a conforma-

* Present address: Materials and Molecular Research Division, Lawrence Berkeley Laboratory, University of California, Berkeley, California 94720, USA.
‡ To whom correspondence should be addressed.

0301-0104/82/0000–0000/$ 02.75

tional cooling effect was found for the former molecule but not for the latter [4]. More recently, Hopkins et al. [5] reported fluorescence excitation spectra of jet-cooled alkylbenzenes showing no evidence of conformal cooling.

In the following we present the results of further experiments with 1,2-difluoroethane (DFE) and methyl nitrite (MEN) as well as with 1,2-dichloroethane (DCE), whose barriers to internal rotation amount to approximately 700, 2800 and 1200 cm^{-1}. These barriers may be qualified as "low", "high" and "medium", and by virtue of the barrier the three molecules may be expected to behave differently with respect to conformational relaxation. The experimental technique rests on the fact that conformational isomers of all three molecules were shown to be trapped into cryogenic argon matrices without alteration of the conformer populations by the deposition process [6–9]. By comparison of IR absorption intensity ratios of matrix-isolated samples deposited from thermal effusive molecular beams with those from supersonic beams, a conformational cooling effect in the latter can be detected. Details are given in section 2. Experimental results will be presented in section 3. In order to rationalize the experimental findings, a fluid dynamical model of conformer interconversion kinetics in supersonic jets is outlined in section 4. In section 5 experimental and computational results are compared and discussed.

2. Experimental

2.1. General

For the experiments to be described here, two types of molecular-beam sources were used in connection with a cryostat–IR spectrometer system. Accordingly, the beam sources were designed in a way to maintain a certain versatility of the system. The various components will be described below.

2.2. Molecular beam sources

The supersonic molecular-beam system is shown in fig. 1. It consists of two cylindrical stainless-steel chambers connected by a rigid tube. The source chamber is pumped by a 5200 ℓ/s^{-1} oil diffusion pump. In order to maximize pumping speed no baffle was used. The stagnation reservoir consists of a 9 mm i.d. tube mounted on an *xyz* translation stage of our own design. The supersonic nozzle is a molybdenum aperture for electron microscopes (Siemens) and is tightened to the stagnation reservoir tube with a copper gasket. Most experiments were done using a 0.1 mm diameter aperture. The core of the supersonic jet is sampled by means of a home-built conical stainless-steel skimmer (0.8 mm diameter, 29 mm high) mounted between source and buffer chamber. The nozzle–skimmer distance can be varied in the range 0–30 mm. Before reaching the exit flange of the apparatus the beam is collimated by a circular 10 mm aperture. A small quadrupole mass spectrometer (Balzers QMA 113) inserted into the buffer chamber slightly above the molecular-beam path allows for monitoring the composition of the beam. A small quartz window at the outside end of the stagnation reservoir can be used to check optically the alignment of the beam-defining elements. With a supersonic beam in operation the pressure was usually around 10^{-4} Torr in the source chamber and below 5×10^{-7} Torr in the buffer chamber.

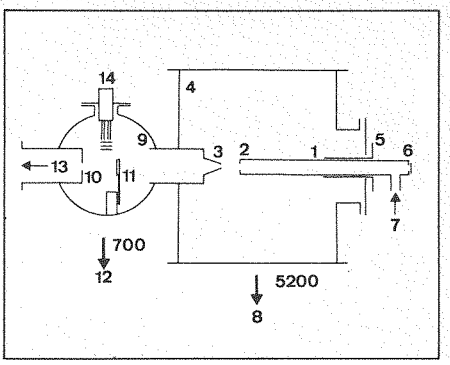

Fig. 1. Supersonic beam apparatus (vertical section). Key: 1 stagnation reservoir, 2 nozzle, 3 skimmer, 4 source chamber, 5 translator flange, 6 window, 7 substance inlet, 8 oil diffusion pump (Balzers DIF 320), 9 buffer chamber, 10 collimator, 11 tuning fork chopper, 12 oil diffusion pump (Edwards Diffstak 160/700 M), 13 molecular beam, 14 mass spectrometer (Balzers QMA 113).

Thermal effusive molecular beams were generated with a heatable Knudsen cell operated in a flow mode [10]. With an orifice diameter of 0.7 mm and a pressure around 10 mTorr the Knudsen number at the exit was sufficiently high to ensure effusive conditions.

2.3. Apparatus for matrix IR spectroscopy

The molecular beams to be investigated were deposited on a CsI target window cooled by a home-built liquid-helium bath cryostat. Argon matrix gas was deposited simultaneously through a separated orifice system. In the case of thermal effusive beam experiments the matrix gas system is mounted onto the Knudsen cell itself, whereas for supersonic beam deposition it is incorporated in the bellows coupler between beam source and cryostat [11]. After deposition of the matrix the cryostat is rotated by 90° and the IR transmission spectrum is recorded with a Perkin–Elmer 325 grating spectrophotometer. For intensity determination absorption bands were recorded in 0.02 cm^{-1} steps with a digital sampling system and processed off-line.

2.4. Chemicals

1,2-difluoroethane (DFE) (96% GC) was purchased from Armaggedon Chemical Corp., Durham, NC (USA); 1,2-dichloroethane (DCE) (99.5% GC) was obtained from Fluka AG, Buchs (Switzerland). Both substances were used without further purification. Methyl nitrite (MEN) was prepared according to a description in the literature [12] and distilled at low temperature prior to use.

Ultrahigh purity argon gas (99.9999%) from Messer Griesheim GmbH, Duisburg (FRG) was used as matrix gas, whereas ordinary (99.995%) argon and helium were used as carrier gases in seeded supersonic beams. Gas mixtures for seeded beams were prepared in a 10ℓ steel bomb. Some low-dilution DCE : argon mixtures were obtained by bubbling argon gas through liquid DCE at 15°C in a gas saturator system.

As mentioned in section 2.2, the constancy of the composition of seeded beams was checked mass spectrometrically.

2.5. Treatment of experimental results

For the conformer interconversion process

$$-A_1 + A_2 = 0\,, \tag{1}$$

the equilibrium constant is given approximately by

$$K(T) = x_2/x_1 = (g_2/g_1)\exp\left[-\Delta H^0(T_r)/RT + \Delta S^0(T_r)/R\right];\ T \approx T_r, \tag{2}$$

with x_i and g_i denoting mole fraction and symmetry number of conformer i. A thermodynamic reference temperature T_r = 298 K has been used throughout this work.

In a thermal effusive molecular beam T is identical with the stagnation temperature T_0. In a supersonic molecular beam we are dealing with an inherently non-equilibrium situation, and the conformer ratio x_2/x_1 will, in general, not be given by inserting $T = T_0$ in (2). If, however, we find an experimental way to determine the conformer ratio in a supersonic beam, we can use eq. (2) in the reverse sense. To any value x_2/x_1 we can assign a conformational temperature T_c. This corresponds to a visualization of a conformer ratio by specifying the temperature at which a system in thermal equilibrium exhibits the same conformer distribution.

As has been mentioned in section 1, this investigation rests on the trapping of conformational isomers during matrix deposition. This means that by intensity measurements of matrix spectra, information on conformer populations in the molecular beam can be obtained. The connection between absorption intensity ratios and conformer population ratios is found by depositing thermal effusive molecular beams at several temperatures. This has already been done for the molecules of this study [6–9]. The method will thus be discussed only briefly.

If the beam molecules are suddenly trapped into the matrix

$$x_2/x_1 = [A_2]/[A_1]\,, \tag{3}$$

where $[A_i]$ is the concentration (mol cm^{-3}) of conformer i in the matrix. Consider now the kth absorption band of the matrix-isolated species i. If overlapping of absorption bands can be neglected, Beer's law states that

$$-\log T(\tilde{\nu}) = \epsilon_{ki}(\tilde{\nu})\,[A_i]\,l\,,\quad \tilde{\nu} \in V_{ki}\,, \tag{4}$$

where $T(\tilde{\nu})$ is the spectral transmittance of the matrix, l is the layer thickness and $\epsilon_{ki}(\tilde{\nu})$ is the spectral molar decadic absorption coefficient. V_{ki} is the wavenumber domain into which the kth band of conformer i is

confined from a practical point of view.

We introduce a normalized lineshape function $f_{ki}(\tilde{\nu})$ and an integrated molar decadic absorption coefficient ϵ_{ki}:

$$-\log T(\tilde{\nu}) = \epsilon_{ki} f_{ki}(\tilde{\nu})\, l\, [\mathrm{A}_i]\,, \tag{5}$$

with

$$\int_{V_{ki}} f_{ki}(\tilde{\nu})\, \mathrm{d}\tilde{\nu} = 1\,. \tag{6}$$

Integration of (4) over the band profile yields the integrated decadic absorbance

$$A_{ki} \overset{\text{def}}{=} -\int_{V_{ki}} \log T(\tilde{\nu})\, \mathrm{d}\tilde{\nu} = \epsilon_{ki}[\mathrm{A}_i]\, l\,. \tag{7}$$

Considering the kth absorption band of A_2 and the lth band of A_1, eqs. (2)–(4) and (7) can be combined to

$$\ln(A_{k2}/A_{l1}) = -\Delta H^0(T_r)/RT + \Delta S^0(T_r)/R + \ln(g_2/g_1) + \ln(\epsilon_{k2}/\epsilon_{l1})\,. \tag{8}$$

In practice the integration in eq. (7) is done using digitalized transmittance spectra (see section 2.3).

The reasons for using integrated absorbances instead of peak absorbances are twofold. Firstly, comparison of integrated absorbances is only slightly influenced by the non-reproducibility of lineshapes in different experiments. Secondly, it should be remembered that all our measurements yield apparent transmittances, i.e. the convolution of the true lineshape with the spectral slit function of the monochromator. As shown by numerical evaluation, this convolution affects ratios of integrated absorbances considerably less than ratios of peak absorbances.

As is seen from eq. (8), linear regression of $\ln(A_{k2}/A_{l1})$ versus T^{-1} allows us to determine the standard enthalpy $\Delta H^0(T_r)$ of the conformer interconversion from the slope. The sum of the last three terms of the rhs of (8) appears as the intercept. Though most often g_2/g_1 is known, this is not the case for $\epsilon_{k2}/\epsilon_{l1}$, so that $\Delta S^0(T_r)$ usually cannot be determined. It is evident that the result of the linear regression can be used backwards to evaluate the molecular-beam temperature corresponding to a measured intensity ratio. This procedure can be applied to supersonic molecular beams in order to evaluate the conformational temperature T_c. In view of relaxation processes which might occur downstream of the beam source, this temperature will, in general, not be identical with the stagnation temperature T_0. From the general behavior of supersonic molecular beams we can safely assume that T_c varies only in a restricted neighborhood of the nozzle. When the molecular beam reaches the matrix target, the conformational temperature has already reached its terminal value T_c^∞.

In section 3 results of T_c^∞ measurements are reported.

3. Results

3.1. 1,3-difluoroethane (DFE)

In a first series of experiments supersonic beams of pure DFE were deposited by using different stagnation conditions. For the determination of conformer ratios the three strong absorption bands between 1100 and 1040 cm^{-1} were recorded. Although data from experiments with thermal effusive beams of DFE were available [6,7], two effusive experiments were repeated in order to record spectra under conditions as similar as possible to those of supersonic beam experiments. From integrated absorbances a value of $\Delta H^0(T_r) = 588$ cal mol^{-1} was found. This is in good agreement with $\Delta H^0(T_r) = 574$ (90) cal mol^{-1} of the previous investigation [7]. Table 1 lists experimental conditions and integrated band intensities, including the results of a preliminary study [4]‡.

In fig. 2 the absorption bands are displayed for some of the experiments listed in table 1. In order to visualize conformer ratios the absorbance scale in each experiment has been normalized to the integrated absorbance of the gauche-DFE band centered near 1070 cm^{-1}. Fig. 2 can be commented on as follows.

(i) The peak height of the band near 1070 cm^{-1} is nearly constant. The scale having been normalized to the integral over the band, it can be concluded that the lineshape is quite constant in all experiments.

‡ Values of integrated absorbances given in ref. [4] have been computed erroneously and should be replaced by those in table 1.

Table 1
Experimental conditions and results of matrix-trapped molecular beams of pure DFE

Molecular beam a)			Matrix b)		Integrated apparent decadic absorbance c)					T_c^{∞} (K) d)
p_0	d_0	z_s	l	m/A	A^g_{1096}	A^g_{1070}	A^t_{1048}	$\frac{A^g_{1096}}{A^g_{1070}}$	$\frac{A^t_{1048}}{A^g_{1070}}$	
450	100	13	285	1800	0.5621	0.3229	0.1130	1.74	0.350	207(3)
300	100	11	335	2100	0.5382	0.3069	0.1150	1.75	0.375	217(3)
300	100	11	275	1600	0.5709	0.3363	0.1232	1.70	0.366	213(3)
200	100	9	360	2200	0.5413	0.3106	0.1376	1.74	0.443	247(4)
100	100	7	550	3500	0.4955	0.2787	0.1420	2.78	0.501	280(5)
T_0 = 23°C		240	1100	1700	0.4373	0.3459	0.1326	1.78	0.539	296
T_0 = 101°C			260	1800	0.4131	0.2330	0.1546	1.77	0.664	374
400	125	4	320	1500	0.5273	0.2999	0.1197	1.76	0.399	220(6)
T_0 = 23°C			300	1500	0.4921	0.2925	0.1657	1.68	0.566	296

a) Supersonic beams; stagnation temperature T_0 = 296 K, stagnation pressure p_0 in Torr, nozzle diameter d_0 in μm, nozzle–skimmer separation z_s in mm. Effusive beams are characterized by the stagnation temperature T_0.
b) Layer thickness l of argon matrix in μm. M/A is the matrix isolation ratio.
c) The superscript refers to the conformer (g = gauche, t = trans), the subscript denotes the band-center wavenumber.
d) Terminal conformational temperature, calculated for ΔH^0 = 588 cal mol^{-1}.

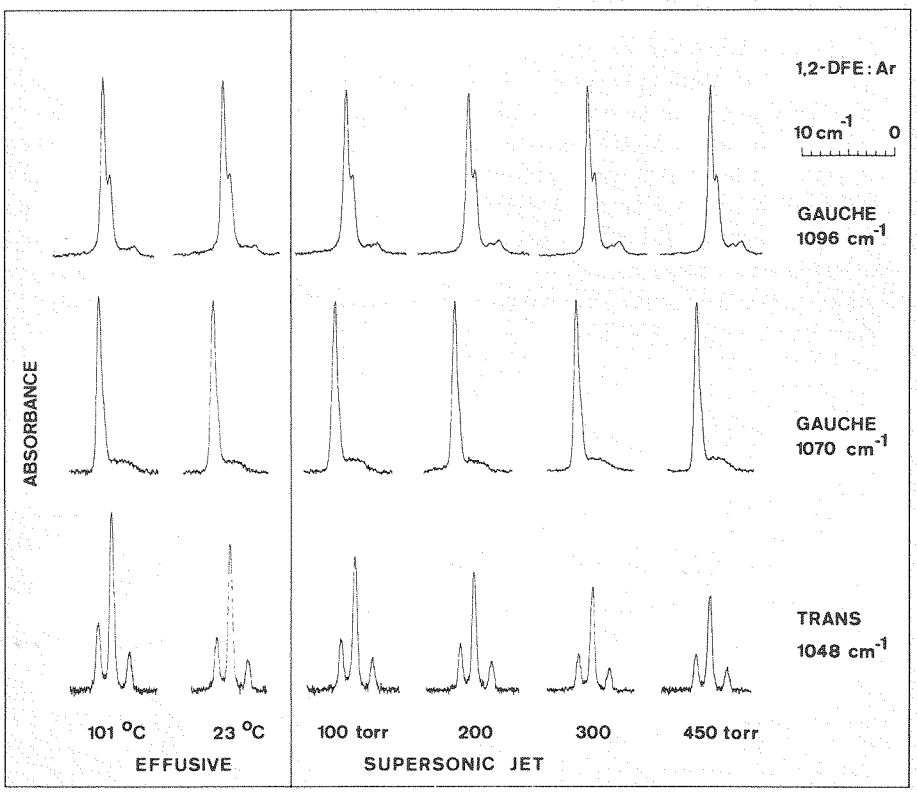

Fig. 2. Intensity comparison of IR absorption bands measured after matrix deposition of molecular beams of pure DFE. For each experiment the three bands in the CF-stretching region are displayed in a column (see table 1 for the experimental conditions). For each row the approximate position of the band center is indicated on the right side. For each experiment the ordinate scales were expanded by a factor which normalizes the integral over the band near 1070 cm^{-1}. Therefore in each row a comparison of relative absorbances is possible.

(ii) The intensity variation of the second band of gauche-DFE near 1096 cm^{-1} gives an estimate of the reproducibility of the intensity measurements.

(iii) The systematic change of the normalized intensity of the absorption band of trans-DFE shows the dependence of the conformer ratio upon the molecular-beam conditions. It is obvious that increasing the supersonic beam stagnation pressure induces a depopulation of the (less stable) trans-DFE conformer.

The last column of table 1 lists terminal conformational temperatures of DFE supersonic beams deduced from the experimental results by using a value $\Delta H^0(T_r) = 588$ cal mol^{-1}. In section 5 these values will be compared to the results of model calculations.

In a second series of measurements DFE was seeded in argon carrier gas. In order to obtain a reasonable DFE deposition rate the seeding ratio had to be kept relatively high (mole fraction in the reservoir $x_{DFE,0} > 0.008$). This resulted in a considerable formation of $(DFE)_n$ clusters, as revealed by the appearance of broad features in the matrix IR spectra (see fig. 3). Table 2 lists experiments with seeded supersonic beams. To obtain integrated absorbances, background corrections were made by assuming a locally quadratic polynomial as baseline. Errors in this correction have a strong influence on the value of the integrated absorbance. Accordingly, it appears difficult to estimate terminal conformational temperatures T_c^∞ of the monomers in seeded supersonic beams. Nevertheless, from the experiment with $p_0 = 1100$ Torr, $d_0 = 100\,\mu$m and Ar : DFE = 125, a slight conformational cooling effect can be inferred, although the associated value $T_c^\infty = 270$ K is to be regarded merely as a rough estimate.

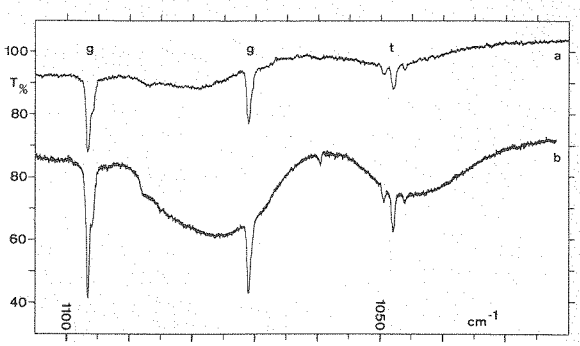

Fig. 3. Matrix spectra obtained after deposition of supersonic beams of DFE seeded in argon. Stagnation conditions spectrum (a): $p_0 = 1100$ Torr, seeding ratio Ar : DFE = 125; spectrum (b): $p_0 = 600$ Torr, Ar : DFE = 10. For the other experimental conditions see table 2.

Finally, one experiment has been performed using a supersonic beam of DFE seeded in helium. Obviously this carrier gas is not condensed into the matrix but is instead pumped off by the vacuum system of the cryostat. With a helium: DFE ratio of 50, stagnation pressure $P_0 = 600$ Torr and nozzle diameter $d_0 = 100\,\mu$m, the matrix spectrum obtained did not show any significant departure from the intensity distribution corresponding to $T_c^\infty = T_0 = 296$ K.

Table 2
Experimental conditions and results of matrix-trapped supersonic beams of DFE seeded in argon or helium

Molecular beam a)			Matrix b)	Integrated apparent decadic absorbance c)				
p_0	z_s	x_{DFE}^{-1}	l	A^g_{1096}	A^g_{1070}	A^t_{1048}	$\frac{A^g_{1096}}{A^g_{1070}}$	$\frac{A^t_{1048}}{A^g_{1070}}$
600	12 Ar	10	400	0.322	0.179	0.099	1.80	0.55
600	12 Ar	50	660	too weak			—	—
1100	14 Ar	55	765	0.204	0.112	0.056	1.82	0.50
1100	14 Ar	125	1375	0.187	0.105	0.052	1.79	0.50
600	7 He	50	210	0.695	0.388	0.220	1.79	0.57

a) Stagnation temperature $T_0 = 296$ K, nozzle diameter $d_0 = 100\,\mu$m, stagnation pressure p_0 in Torr, nozzle–skimmer separation z_s in mm, carrier gas, seeding ratio x_{DFE}^{-1}.
b) Layer thickness l of argon matrix in μm.
c) The superscript refers to the conformer (g = gauche, t = trans), the subscript denotes the band-center wavenumber.

3.2. Dichloroethane (DCE) and methyl nitrite (MEN)

For both molecules several matrix-deposition experiments have been undertaken. No evidence of a significant depopulation of the less stable conformers gauche-DCE [8] and trans-MEN [9] by the supersonic expansion has been found.

In the case of DCE the relatively low vapor pressure at room temperature limits the stagnation pressure for pure beams to ≈65 Torr. With seeded beams of DCE in argon considerable aggregation was found in the low-dilution range, i.e. $0.5 < x_{DCE,0} < 0.3$. At higher dilution ($x \leqslant 0.02$) experiments were hampered by the weakness of those absorption bands which are suitable for intensity determinations. A typical matrix spectrum of DCE obtained after deposition of a seeded supersonic argon beam is shown in fig. 4.

Matrix spectra of MEN from supersonic beams are easier to obtain owing to the very strong IR spectra of both cis- and trans-MEN. Moreover, MEN shows only little tendency to form clusters both in pure and in seeded beams. Three representative experiments are presented in fig. 5 and in table 3. From experiment B (MEN seeded in Ar) a slight conformational cooling effect might be inferred, but the evidence is

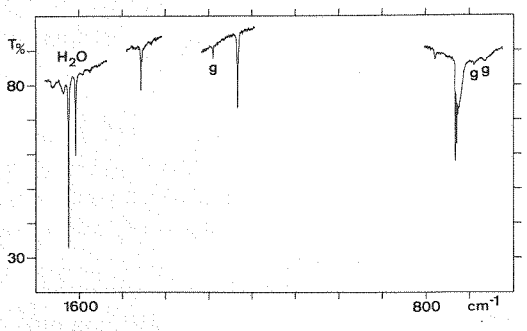

Fig. 4. Matrix spectrum obtained after deposition of a supersonic beam of DCE seeded in argon. Stagnation conditions: T_0 = 296 K, p_0 = 300 Torr, d_0 = 100 μm, Ar : DCE = 38. Matrix layer thickness 675 μm, deposition time 7.5 h. Absorption bands of the less stable gauche conformer are labelled "g", whereas "H_2O" denotes absorption bands of water in the argon matrix.

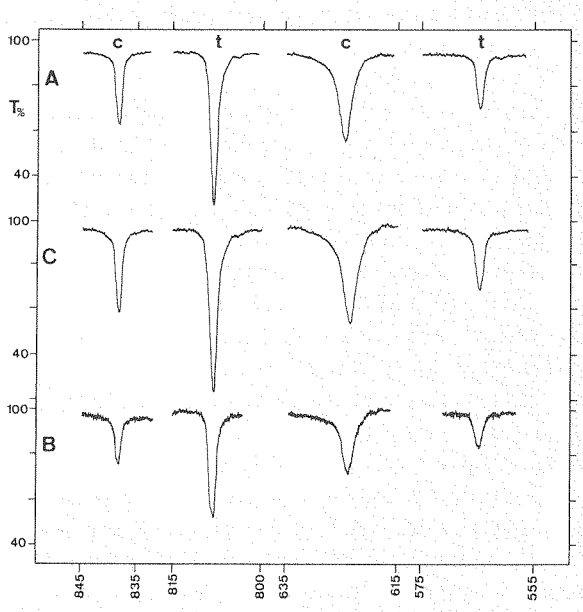

Fig. 5. Matrix spectra obtained after deposition of molecular beams of MEN. (A) Supersonic beam of pure MEN. (B) Supersonic beam of MEN seeded in argon carrier. (C) Thermal effusive beam of pure MEN. The experimental conditions leading to spectra (A), (B) and (C) are summarized in table 3.

Table 3
Experimental conditions and results of matrix-trapped molecuarl beams of MEN

Molecular beam a)					Matrix b)		Apparent decadic peak absorbance c)					
	p_0	d_0	z_s	x^{-1}_{MEN}	l	M/A	A^c_{838}	A^t_{807}	A^c_{625}	A^t_{565}	$\frac{A^t_{807}}{A^c_{828}}$	$\frac{A^t_{565}}{A^c_{625}}$
A	400	50	4 – Ar	1	200	2300	0.179	0.538	0.228	0.133	3.00	0.58
B	200	200	14 – Ar	70	675	7800	0.105	0.279	0.137	0.069	2.66	0.50
C	T_0 = 23°C		effusive	110	110	1200	0.215	0.625	0.251	0.143	2.91	0.57

a) Supersonic beams: stagnation temperature T_0 = 296 K, stagnation pressure p_0 in Torr, nozzle diameter d_0 in μm, nozzle–skimmer separation z_s in mm, carrier gas, seeding ratio x^{-1}_{MEN}.
b) Layer thickness l of argon matrix in μm, M/A is the matrix isolation ratio.
c) The superscript refers to the conformer (c = cis, t = trans), the subscript denotes the band-center wavenumber.

not conclusive in view of the uncertainty of the intensity measurements.

4. Model calculations

4.1. Model

Before introducing a model to describe the kinetics of conformer interconversions in a continuum free jet, a brief review of related investigations by other authors should be given.

(i) Cooling of rotational and vibrational degrees of freedom in supersonic jets has been treated mainly by two methods. Both approaches begin by assuming a stationary continuum flow. The values of the flow-field variables (temperature T, particle density n, flow velocity u) characterize the frame in which local rate equations are set up in the temporal domain. In one method the relaxation kinetics are formulated in terms of molecular energy-level populations [3,13]. In a second method, often called a thermal-conduction model, relaxation equations for the internal temperatures T_i associated with the populations of molecular energy levels E_i [15–18] are used.

If velocity slip can be neglected, the temporal equations can easily be transformed into the spatial domain by use of the flow velocity. It is important to note that in the models mentioned above the flow field is used to determine the parameters T, n, u for the rate problem. The influence of the internal-energy exchange to the local heat bath formed by the flow field is assumed to be negligible **.

(ii) Chemical relaxation in free jets has been discussed by Knuth [20] in terms of a sudden-freeze model and applied to dimerization reactions [21]; the method has also been used for vibrational relaxation [22]. By introducing a criterion of consecutive freezing the relaxation of several degrees of freedom can be incorporated into the model calculations.

Bergmann et al. [23] have studied the dimerization of sodium atoms and taken into account the release of binding energy to the flow field but without explicitly formulating kinetic equations in the whole flow field.

We now turn to our model of conformational interconversions in free-jet expansions. By virtue of the fact that we are dealing with a type of chemical reaction in which the number of particles is conserved, we can adopt a formulation similar to those mentioned for vibrational relaxation problems ‡‡.

We consider an isentropic, stationary, laminar, inviscid flow field consisting of a monatomic carrier gas M and of a molecular species A, featuring conformers A_1 and A_2. Local particle densities of these species will be denoted n_M, n_1 and n_2, respectively. In addition to the fluid dynamical processes we introduce the kinetics of the conformal exchange reaction (1) and describe it by a local equation of motion (with $n_i = n_i(x, t)$):

$$(\partial n_2/\partial t)_{\text{chem}} = -(\partial n_1/\partial t)_{\text{chem}} , \tag{9}$$

with the partial derivative referring to a fixed location x in the stationary flow field.

We explicitly note that

(i) the release of reaction energy is assumed to have a negligible effect on the temperature of the local heat bath formed by the translational (and possibly rotational and vibrational) degrees of freedom of the gas mixture components;

(ii) by using a description based on continuum fluid dynamics the conformer interconversion process is assumed to take place in the collision-dominated part of the jet flow and to freeze out before the onset of rarefaction effects.

These two points will be discussed briefly in section 5.

If diffusion is negligible, the particle density of species i obeys the conservation equation (see appendix C)

$$(\partial n_i/\partial t)_{\text{chem}} - \nabla(u n_i) = 0 , \tag{10}$$

where u denotes the flow velocity. In the special cases $n_i = n_M, n_i = n_A = n_1 + n_2$ and $n_i = n = n_A + n_M$, the first term in (10) is zero, reflecting the fact that the carrier gas particle density as well as the total seed

** For a self-consistent treatment see e.g. Anderson [19], whose method, however, requires a specified nozzle shape, ~~but seems nevertheless applicable to free jets of the type used in this work.~~ and is not applicable to free jets.

‡‡ A conceptual difference between conformational and vibrational or rotational relaxation lies in the fact that "conformers" are not single quantum states. A conformer represents a manifold of molecular eigenstates localized near a minimum of the molecular energy surface.

particle density are chemical invariants in the case of isomerization reactions. This leads to the usual continuity equation of fluid dynamics

$$\nabla(un) = 0 \,. \tag{11}$$

For convenience we introduce the following dimensionless quantities:

$$x = (n_1 + n_2)/(n_1 + n_2 + n_M) = n_A/n \,, \tag{12}$$

$$q = n_2/(n_1 + n_2) = n_2/n_A \,. \tag{13}$$

The parameter x corresponds to the mole fraction of the seed in the gas mixture. In the model considered here x is constant throughout the flow field. The variable q specifies the relative population of the less stable conformer A_2. Inserting (12) and (13) into (10) and considering a narrow streamline along the molecular-beam axis z yields

$$(\partial q/\partial t)_{chem} - u_z \, \partial q/\partial z = 0 \,, \tag{14}$$

where u_z is the flow velocity in the z direction. In this general form eq. (14) does not apply to conformer exchange only, but also to the dynamics of other processes in which the total particle number is left invariant. The detailed feature of the phenomena under investigation is expressed by specifying the form of the "reaction rate" $(\partial q/\partial t)_{chem}$.

Assuming bimolecular elementary processes

$$A_1 + M \underset{k_{-1}}{\overset{k_{+1}}{\rightleftharpoons}} A_2 + M \,, \tag{15}$$

$$A_1 + A_i \underset{k_{-2}}{\overset{k_{+2}}{\rightleftharpoons}} A_2 + A_i \quad (i = 1 \text{ or } 2) \,, \tag{16}$$

leads to

$$(\partial q/\partial t)_{chem} = n[k_{+1}(1-q)(1-x) + k_{+2}(1-q)x - k_{-1}q(1-x) - k_{-2}qx] \,. \tag{17}$$

An estimation of the reaction rate constants k using a bimolecular collision model is outlined in appendix A. This allows to write the rate constant as a function of the local values of temperature, particle density and conformer ratio:

$$(\partial q/\partial t)_{chem} = Q(T, n, q) \,, \tag{18}$$

with Q denoting the right-hand side of eq. (17).

Eq. (14) can now be written as

$$\partial q/\partial z = (1/u_z)\, Q(T, n, q) \,. \tag{19}$$

In order to integrate (19) the values of the flow-field variables u_z, T and n should be expressed as functions of the spatial coordinate z. This is easily accomplished via the well-known isentropic relations, provided that the Mach number Ma is known as a function of z. In the present calculation the spatial dependence of Ma has been estimated by using the approximations presented in appendix B.

The problem to be solved has thus been reduced to the differential equation

$$\partial q/\partial z = (1/u_z)\, Q(q, z) \,, \tag{20}$$

subject to the initial condition

$$q(z_0) = q_0 \,. \tag{21}$$

The boundary conditions are represented by the spatial dependence of the Mach number, by the isentropic relations and by the kinetic mechanisms considered. As initial condition (21) it is assumed that near $z \leqslant z_0$ the conformer distribution q obeys thermodynamic equilibrium at stagnation conditions.

The integration of (20) can be performed numerically using a scheme as visualized in fig. 6. For the actual calculations a FORTRAN IV program using an eight-order Runge–Kutta subroutine with stepsize control [24] has been written. As detailed in appendix A, calculated values of q can be transformed to the conformational temperature T_c in order to facilitate comparison with experimental results.

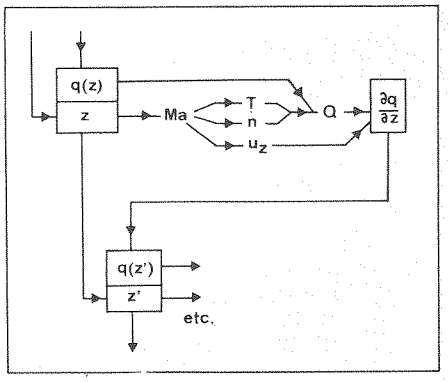

Fig. 6. Numerical integration method used in the model calculations (see text). From the values z and $q(z)$ the spatial derivative $\partial q/\partial z$ is evaluated according to eq. (20). The value $q(z')$ at a new location $z' = z + \Delta z$ is calculated by means of a difference scheme.

Table 4
Values of molecular parameters kept fixed in all calculations

		DFE	DCE	MEN	Argon
molar mass [a]	M	66.05	98.96	61.04	40.00
more stable conformer	A_1	gauche	trans	cis	–
less stable conformer	A_2	trans	gauche	trans	–
symmetry number	g_1	2	1	1	–
	g_2	1	2	1	–
reaction enthalpy [b]	ΔH^0	588	1040	623	–
activation energy [b,c,d]	$E_-^{\ddagger}$	2000	3300	8000	–
specific heat ratio	γ	1.15	1.15	1.15	1.667

a) g mol^{-1}. b) cal mol^{-1}. c) For reaction $A_2 \rightarrow A_1$.
d) Assumed as equal to the internal rotation barrier, see text.

4.2. Computational results

Before presenting results of model calculations we note that the values of some molecular parameters have been kept fixed in all computations. These are summarized in table 4. The reaction enthalpies have been taken from the results of thermal effusive beam investigations (DFE: see section 3, DCE: see ref. [8], MEN: see ref. [9]). The reaction entropies have been set to zero. The activation energies were estimated from the heights of the corresponding energy barriers of the internal rotation potentials, the latter having been taken from the literature (for DFE and MEN: see ref. [4], for DCE: see ref. [25]). The ratio of specific heat capacities $\gamma = C_p/C_V$ has been set equal to 1.15 for all molecular species[‡‡] and to 5/3 for argon. Therefore in all calculations only the values of effective reactive impact parameters were left as adjustable quantities.

Table 5 gives a comparison of measured and of calculated terminal conformational temperatures in supersonic jets of pure DFE and MEN. For DFE expansions the choice of $\sigma^2_{DFE,DFE} = 50$ Å^2 reproduces the experimental data at higher stagnation pressures (see also fig. 7). At lower pressures the cooling effect

[‡‡] In a statistical thermodynamic calculation of DFE using the rigid rotor, harmonic oscillator approximation, the following γ values were found: γ (gauche; 298 K) = 1.148, γ(gauche; 150 K) = 1.212, γ(trans; 298 K) = 1.141, γ(trans; 150 K) = 1.219.

Table 5
Supersonic expansions of pure DFE and of pure MEN: Comparison of experimental and calculated terminal conformational temperature

p_0 [a]	T_c^{∞} (DFE) [b,c]		T_c^{∞}(MEN) [b,d]	
	experimental	calculated [e]	experimental	calculated [f]
25		259		
50		247		
100	280 (5)	234		
200	247 (4)	221		
300	215 (3)	214		
400			296	296
450	207 (3)	206		
900		195		

a) Stagnation pressure in Torr. Stagnation temperature $T_0 = 296$ K. b) Terminal conformational temperature in Kelvin.
c) Nozzle diameter $d_0 = 100$ μm. d) $d_0 = 50$ μm. e) $\sigma^2_{DFE,DFE} = 50$ Å^2. f) Using $\sigma^2_{MEN,MEN} = 100$ Å^2.

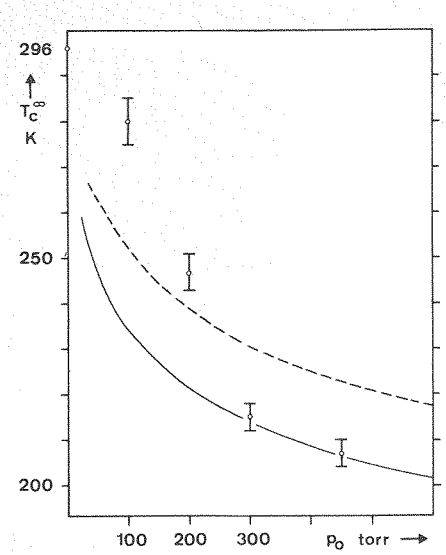

Fig. 7. Terminal conformational temperature T_c^∞ in supersonic beams of pure DFE. Dependence of T_c^∞ on the stagnation pressure p_0 for fixed values $d_0 = 100\,\mu m$, $T_0 = 296$ K. Circles indicate measured values (see table 1); full line: model calculation (see section 4) using $\sigma^2_{DFE,DFE} = 50$ Å^2, dashed line: calculated using $\sigma^2_{DFE,DFE} = 20$ Å^2.

predicted by the calculations with this value of $\sigma^2_{DFE,DFE}$ is too strong, but by lowering its value, better agreement is obtained. In fig. 8 the conformational and translational temperatures in an expansion of pure DFE are plotted versus the distance from the nozzle. It is evident that the conformer distribution starts lagging behind the translational temperature shortly after the nozzle exit.

In the case of MEN the absence of a conformational cooling effect is confirmed by the model calculations even when the magnitude of $\sigma^2_{MEN,MEN}$ is deliberately exaggerated.

For the discussion of mixed gas expansions the effective impact parameter for reactive collisions between carrier and seed molecules has to be introduced as an additional quantity. As documented in table 6 the results found for DFE : argon suggest that collisions between DFE and Ar are negligible if $\sigma^2_{DFE,DFE}$ is to be kept at a value of 50 Å^2 as deduced from the results of pure DFE jets. In the case of DCE and MEN seeded in argon, no significant conformational cooling is predicted from the calculations, thus confirming the experimental findings. These results will be discussed in section 5.

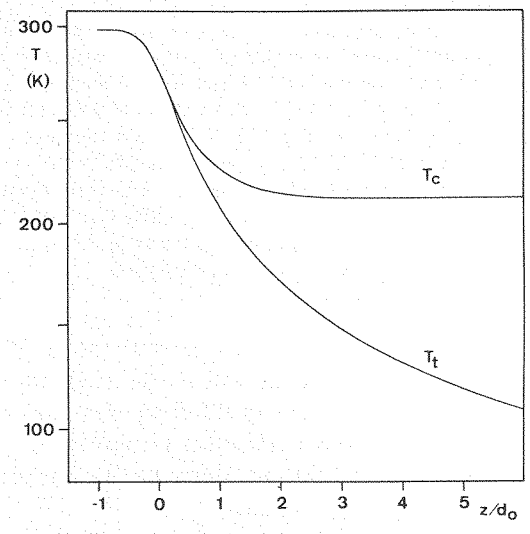

Fig. 8. Spatial dependence of conformational temperature T_c and of translational temperature T_t calculated for a continuum free jet of pure DFE. ($p_0 = 450$ Torr, $d_0 = 100\,\mu m$, $T_0 = 296$ K, $\sigma^2_{DFE,DFE} = 50$ Å^2.) z is the axial distance from the nozzle exit plane.

Table 6
Supersonic expansions of DFE : Ar, DCE : Ar and MEN : Ar mixtures: Comparison of experimental and calculated terminal conformational temperatures

		T_c^∞(DFE) [a,b]	T_c^∞(DCE) [a,c]	T_c^∞(MEN) [a,d]
calculated using [e]				
σ^2_{AA}	σ^2_{AM}			
50	0.1	261	–	–
50	0.0	269	–	–
100	1.0	–	289	296
100	10	–	274	296
experimental		270	296	296

[a] Terminal conformational temperature in Kelvin.
[b] $p_0 = 1100$ Torr, $d_0 = 100\,\mu m$, $T_0 = 296$ K, Ar : DFE = 125.
[c] $p_0 = 200$ Torr, $d_0 = 200\,\mu m$, $T_0 = 296$ K, Ar : DCE = 40.
[d] $p_0 = 200$ Torr, $d_0 = 200\,\mu m$, $T_0 = 296$ K, Ar : MEN = 70.
[e] Square of effective reactive impact parameters, in Å^2. The first column refers to intermolecular collisions, the second column to molecule–carrier gas collisions.

5. Discussion

It seems natural to begin this section with an assessment of the "conformer-trapping assumption". Obviously the assumption that conformational distributions of molecular beams are trapped into the argon matrix is crucial for the interpretation of the results presented in section 3. First of all it should be noted that for the molecules of this investigation trapping of conformers has been found for thermal effusive beams [6–9]. Moreover, no conformational interconversions induced by the globar source of the spectrometer were found to take place even after several hours of measurement.

In the case of supersonic molecular beams departures from ideal conformer trapping might be expected for molecules hitting the target at high impact velocity. In fig. 9 the relative current density at the target has been plotted versus the kinetic energy for molecular beams of DFE. The beam conditions in fig. 9 are believed to qualitatively represent the experiments described in section 3, although measurements of velocity distributions have not been undertaken.

Comparison of the values determined for T_c^∞ with the plots in fig. 9 indicates that conformer trapping is achieved even at high impact energies. This is best seen in the case of DFE seeded in helium, which features a strongly hyperthermal velocity distribution of the seed molecules but shows the same conformer ratio as a room-temperature effusive beam (cf. table 2).

Another error source in the determination of T_c^∞ might arise from collisions between supersonic-beam molecules and argon atoms of the matrix gas inlet. This should result in a shift of the apparent T_c^∞ towards room temperature. Although such an effect cannot be ruled out strictly, it is felt to be negligible mainly for three reasons. Firstly, a corresponding effect has not been found in effusive beam experiments, although geometrical arrangements and beam intensities were quite similar. Secondly, the pressure in the cryostat during matrix deposition was kept below 2×10^{-4} Torr so that the mean free path length was considerably longer than the flight distance in the cryostat. Thirdly, as found from seeded beam experiments, collisions between argon atoms and molecules are inefficient in promoting conformer interconversions.

In view of the above it seems justificable to compare

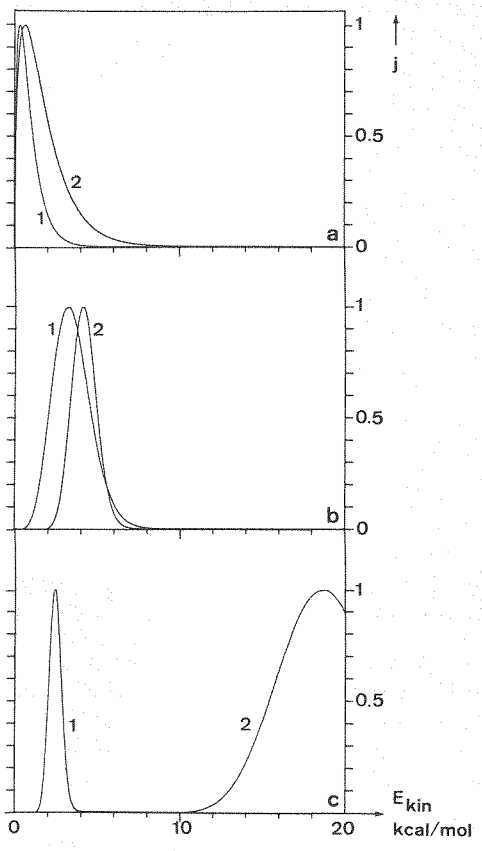

Fig. 9. Probability distribution of DFE current density j (in arbitrary units) plotted versus kinetic energy of impact on a target on beam centerline. (a) Thermal effusive beams, stagnation temperature T_0 = 298 K (curve 1) and 600 K (curve 2). (b) Supersonic beams of pure DFE, T_0 = 298 K, terminal parallel Mach number $Ma_\parallel^\infty$ = 5 (curve 1) and $Ma_\parallel^\infty$ = 10 (curve 2). (c) Seeded supersonic beams of DFE with terminal parallel Mach number $Ma_\parallel^\infty$ = 10 and T_0 = 298 K, 2% DFE in argon (curve 1) and 2% DFE in helium (curve 2). Note that the impact energy refers to the DFE component.

the results of the model calculations with the experimental results. It can be said that all the important experimental findings were qualitatively reproduced by the model description, although a quantitative reproduction was not achieved. Moreover, the following comments should be made.

(i) As was to be expected, the height of the potential barrier between two conformers is the key parameter determining the amount of conformational cooling by supersonic expansion. This fact is well illustrated by the two molecules DFE and MEN, which

are very similar to each other in size and relative stability of the two conformers. The absence of conformational cooling in MEN is almost certainly attributable to the high barrier to internal rotation from trans- to cis-MEN, acting in effect as an activation barrier. In DFE the conformational interconversion rate is much larger owing to the lower internal rotation barrier, and therefore local conformational equilibrium is maintained in the early stages of the supersonic expansion.

(ii) Collisions between two molecules are much more efficient than those between a molecule and a rare-gas atom. A similar behavior has been found in experiments on vibrational relaxation [3]. This might also explain why Hopkins et al. [5] did not find a conformational relaxation of the alkyl chains in supersonic jets containing alkyl benzenes highly diluted in helium carrier gas.

(iii) The early freezing of conformational temperature in all cases examined justifies on one hand the use of continuum mechanics in the model calculations. The onset of rotational and translational freezing effects should lie in a region of the flow field where the conformational temperature has already reached its terminal value. On the other hand, as seen in fig. 8 for DFE, conformational freezing may occur in the transonic domain, i.e. in a region where the flow field is difficult to describe quantitatively.

(iv) In the model presented in section 4, the release of reaction energy due to conformer interconversion was assumed to have negligible influence on the values of the flow-field variables n, u_z and T. The flow field was described as a continuum isentropic expansion of an ideal-gas mixture. Therefore Bernoulli's equation must be valid:

$$C_p T_0 = C_p T + \bar{M} u_z^2 , \tag{22}$$

where $\bar{M}$ is the average molar mass of the gas mixture. The molar specific heat at constant pressure

$$C_p(T) = (\partial H(T)/\partial T)_p , \tag{23}$$

was assumed to be constant throughout the expansion. If, however, the conformer interconversion is taken into account, C_p will contain a contribution

$$C_p'(T) = (\partial H(T)/\partial q)_p (\partial q(T)/\partial T)_p$$
$$= \Delta H^0(T) (\partial q(T)/\partial T)_p . \tag{24}$$

The use of our simplified model is justified provided that

$$C_p' \ll C_p . \tag{25}$$

Obviously the omission of C_p' is questionable particularly in the case of pure substance jets with strong conformational cooling. We can thus limit our considerations to the case of pure DFE jets. If we assume a constant reaction enthalpy $\Delta H^0(T) = \Delta H^0(T_r)$, the maximum value of C_p' is attained at a temperature T_{max} where

$$(\partial q(T)/\partial T)_p \to \max \quad \text{for } T = T_{max} . \tag{26}$$

At this temperature a unit change in temperature induces a maximum change in conformational composition. For DFE, with $\Delta H^0 = 588$ cal mol^{-1}, it is found that $T_{max} \approx 130$ K, with $C_p'(T_{max}) \approx 0.5$ cal mol^{-1} K^{-1}. A lower limit to C_p is given by the sum of the translational and rotational contributions so that for a polyatomic molecule $C_p \geqslant 4R \approx 8$ cal mol^{-1} K^{-1}. Therefore in (25) C_p' is always smaller than 6% of C_p.

In our calculations the criterion (25) is fulfilled to a better degree because the total heat capacity of DFE is certainly larger than $4R$ owing to vibrational contributions. Moreover, the maximum value of C_p' is not reached because the lowest conformational temperatures obtained were around 200 K. This means that the simplified model presented in section 4 is reasonable in the application range discussed here.

We can summarize the results of the present investigation by noting that conformational cooling in supersonic expansions seems to be an exception rather than a rule. Therefore it is not expected that the supersonic-beam technique with stagnation pressures $p_0 \leqslant 2$ atm will be widely applied to simplify matrix IR spectra complicated by the presence of several conformers. By the application of higher stagnation pressures it is, however, not excluded that conformational cooling even with molecules featuring rotational barriers $\geqslant 1000$ cm^{-1} may be achieved. Conversely, however, in a generic supersonic-beam experiment an inefficient conformational relaxation can be an advantage in that observations are not limited to the most stable conformation of a molecule.

Acknowledgement

The authors wish to thank the Swiss National Foundation (Projects No. 2.712–0.77, 2.033–0.78, 2.219–0.79, 2.612–0.80, 2.079–0.81), the ETHZ administration (Project TH 51-0430.5/76) and Mssrs. Sandoz, Basle, for financial support. Introduction to molecular-beam techniques by Professor J.P. Toennies, Max-Planck Institut für Strömungsforschung, Göttingen and by Professor A. Dymanus, Katholieke Universiteit Nijmegen is gratefully acknowledged. Furthermore we wish to thank Mssrs. O. Diener and B. Frei from the laboratory technical staff for construction of the molecular-beam source, Mr. N. Schwizgebel for preparation of methyl nitrite and Mr. H.Z. Zivi for valuable discussions.

Appendix A: Reaction rate

Use a of collision model for bimolecular events leads to a rate constant [26]

$$k = (8\pi kT/\mu_{ik})^{1/2}\,\sigma_{ik}^2 \exp(-E^{\ddagger}/RT)\,, \qquad (A.1)$$

where μ_{ik} is the reduced mass of the colliding pair i, k. $E^{\ddagger}$ is the activation energy and σ_{ik} is an effective impact parameter for reactive collisions. In concomitance with the semiquantitative status of our model we tried to use as few adjustable parameters as possible. We explicitly assumed that

(i) The reaction enthalpy and the activation energy are temperature independent. Denoting as $E_-^{\ddagger}$ the activation energy for the conversion starting from the less stable conformer A_2, it follows immediately that the activation energy of the reverse reaction from A_1 to A_2 is given by $E_+^{\ddagger} = E_-^{\ddagger} + \Delta H^0(T_r)$.

(ii) The reaction entropy is assumed to consist only of the contributions by the degeneracy factors g_1 and g_2.

As specified in section 5 the value $E_-^{\ddagger}$ and $\Delta H^0(T_r)$ can be estimated from experimental values and will therefore be kept fixed. Values of the effective impact parameter are more difficult to estimate; in the calculations they have been varied systematically. The reaction rate constants for the kinetic scheme (7), (8), section 4 are thus

$$k_{+1} = (8\pi kT/\mu_{AM})^{1/2}\sigma_{AM}^2 g_2 \times \exp\{-[E_-^{\ddagger} + \Delta H^0(T_r)]/RT\}\,, \qquad (A.2)$$

$$k_{+2} = 2(\pi kT/m_A)^{1/2}\sigma_{AA}^2 g_2 \times \exp\{-[E_-^{\ddagger} + \Delta H^0(T_r)]/RT\}\,, \qquad (A.3)$$

$$k_{-1} = (8\pi kT/\mu_{AM})^{1/2}\sigma_{AM}^2 g_1 \exp(-E_-^{\ddagger}/RT)\,, \qquad (A.4)$$

$$k_{-2} = 2(\pi kT/m_A)^{1/2}\sigma_{AA}^2 g_1 \exp(-E_-^{\ddagger}/RT)\,, \qquad (A.5)$$

where m_A is the molecular mass of the seed, μ_{AM} is the reduced mass of the seed–carrier pair and g_i are the degeneracies of the reaction channels, i.e. of the isomerization products. It is easy to verify that the thermodynamic limit of the isomerization kinetics is consistently given by

$$(n_2/n_1)_{equil} = (g_2/g_1)\exp[-\Delta H^0(T_r)/RT]\,. \qquad (A.6)$$

Moreover it is useful to note here that the conformational temperature T_c corresponding to a calculated value of the dimensionless variable q is

$$T_c = \frac{\Delta H^0(T_r)}{R \ln[g_2(1-q)/g_1 q]}\,. \qquad (A.7)$$

Appendix B: Approximative description of the flow field

The difficulty in establishing a relation between Mach number and distance form the nozzle lies in the fact that for thin-plate orifice flow no analytic expressions covering the whole range from subsonic to highly supersonic conditions are available. We therefore adopted a piecewise description of the flow field. This method was introduced by Gallagher and Fenn [14] and by Sharma et al. [22] and has subsequently been used with some modifications by other authors [3,13,16,17,23]. Our approach follows closely the one of Quah et al. [16,17] in which four Mach-number regimes are connected together smoothly. In the following we list the expressions for the function Ma(ξ) for the four domains

$$-1 < \xi \leqslant 0,\ 0 < \xi \leqslant \xi_1,\ \xi_1 < \xi \leqslant \xi_2,\ \xi > \xi_2\,,$$

where $\xi = z/d_0$ is the dimensionless axial distance from the nozzle exit plane.

(i) In the highly supersonic region far downstream from the nozzle ($\xi > \xi_2$), we used the well-known results of Ashkenas and Sherman [27] derived by the method of characteristics

$$\mathrm{Ma}(\xi) = A(\xi - \bar{\xi})^{\gamma-1} - [(\gamma+1)/2A(\gamma-1)](\xi-\bar{\xi})^{1-\gamma}\,. \qquad (B.1)$$

The values of the empirical parameters A and $\bar{\xi}$ depend on γ. According to Knuth [20] the following relation holds approximately:

$$A = \{2.2/[(\gamma-1)\gamma]^{1/2}\}^{(\gamma-1)/2}[(\gamma+1)/(\gamma-1)]^{(\gamma+1)/4}. \quad \text{(B.2)}$$

The values of $\bar{\xi}$ have been calculated using

$$\bar{\xi} = 4.74\gamma^2 - 15.70\gamma + 13.08\,, \quad \text{(B.3)}$$

which reproduces the values listed by Anderson [1].

(ii) For the transonic region starting immediately downstream of the orifice ($0 < \xi \leqslant \xi_1$) the results of Knuth's temperature gradient method [20] was used:

$$\mathrm{Ma}(\xi) = \left[\frac{2}{1-\gamma} + \frac{\gamma+1}{\gamma-1}\exp\left(4\xi\frac{\gamma-1}{\gamma+1}\right)\right]^{1/2}, \quad \text{(B.4)}$$

which yields

$$\mathrm{Ma}(\xi=0) = 1\,, \quad (\partial\mathrm{Ma}/\partial\xi)_{\xi=0} = 2\,. \quad \text{(B.5)}$$

(iii) In the region between transonic and highly supersonic flow ($\xi_1 < \xi \leqslant \xi_2$) the Mach number was calculated with a cubic-spline interpolation. In all calculations ξ_1 and ξ_2 were kept as 0.5 and 3.5 respectively. As expected from the behavior of spline functions the interpolation result is quite insensitive to the choice of the limits ξ_1 and ξ_2.

(iv) In the subsonic region $-1 < \xi \leqslant 0$ the quadratic expression

$$\mathrm{Ma}(\xi) = \xi^2 + 2\xi + 1\,, \quad \text{(B.6)}$$

obeying (5) was chosen.

With the expressions listed above the Mach number is specified at every $\xi > -1$, for arbitrary values $\gamma > 1$. We note here that for a binary ideal-gas mixture the ratio of specific heats is given by

$$\bar{\gamma} = \frac{x_A\gamma_A/(\gamma_A-1) + x_B\gamma_B/(\gamma_B-1)}{x_A/(\gamma_A-1) + x_B/(\gamma_B-1)}\,. \quad \text{(B.7)}$$

The values of the flow-field variables temperature, particle density and flow velocity can be calculated from the Mach number by using the isentropic relations

$$T = T_0[1 + \tfrac{1}{2}(\gamma-1)\mathrm{Ma}^2]^{-1}\,, \quad \text{(B.8)}$$

$$n = n_0[1 + \tfrac{1}{2}(\gamma-1)\mathrm{Ma}^2]^{-1/(\gamma-1)}\,, \quad \text{(B.9)}$$

$$u_z = a_0\mathrm{Ma}[1 + \tfrac{1}{2}(\gamma-1)\mathrm{Ma}^2]^{-1/2}\,, \quad \text{(B.10)}$$

with T_0, n_0 and a_0 denoting temperature, particle density and sonic velocity at stagnation conditions.

This completes our approximative description of the flow field. It should be emphasized that though being reliable in the range $\gamma \geqslant 9/7$, the approximation is rather crude for smaller values of γ.

Appendix C: Phenomenological conservation laws for flow fields with chemical reactions

In this appendix the conservation laws concerning the model presented in section 4 are given in a notation commonly adopted in chemical engineering and physical chemistry. Local conservation laws will be formulated for a fixed volume domain G with boundary ∂G within the flow field. For each species $\mathrm{A}_i (i = 1, 2 \ldots A)$ the concentration, molar internal energy function and flow velocity will be denoted by $[\mathrm{A}_i]$, E_i and $\boldsymbol{u}_i$, respectively. These quantities, as well as the flow-field variables will be considered as functions of coordinate vector $\boldsymbol{x}$ and time t. R chemical reactions characterized by stoichiometric equations

$$\sum_{i=1}^{A} \nu_{ji}\mathrm{A}_i = 0, \quad j = 1, \ldots R\,, \quad \text{(C.1)}$$

will be taken into account; the associated rate equations for forward and backward processes (subscript + and −, respectively) read

$$\dot{\xi}_{+j} = k_{+j}\prod_{i=1}^{A}[\mathrm{A}_i]^{\nu_{ji}^-}\,, \quad \text{(C.2)}$$

$$\dot{\xi}_{-j} = k_{-j}\prod_{i=1}^{A}[\mathrm{A}_i]^{\nu_{ji}^+}\,, \quad \text{(C.3)}$$

with

$$\nu_{ji}^{\pm} = \tfrac{1}{2}(|\nu_{ji}| \pm \nu_{ji})\,. \quad \text{(C.4)}$$

The rate constants k will be considered as functions of T, solely. The reaction velocity of concentration $[\mathrm{A}_i]$ is given by

$$[\dot{\mathrm{A}}_i]_{\mathrm{chem}} = \sum_{j=1}^{R}(\dot{\xi}_{+j} - \dot{\xi}_{-j})\nu_{ji}\,. \quad \text{(C.5)}$$

For the following discussion, the rate equations will be assumed to hold locally, although both fields

$T(x, t)$ and $[A_i]\,(x, t)$ are strongly inhomogeneous. The conservation law for any particle A_i then reads

$$-\int_{\partial G}(J_i, \mathrm{d}f) + \int_G [\dot{A}_i]_{\mathrm{chem}}\,\mathrm{d}\tau = \frac{\mathrm{d}}{\mathrm{d}t}\int_G [A_i]\,\mathrm{d}\tau\,, \qquad \text{(C.6)}$$

where J_i is the current density of A_i (moles per unit area and time) and where $\mathrm{d}f$ and $\mathrm{d}\tau$ denote the surface and volume element of the domain G. Applying Gauss' theorem to (C.6) leads to

$$-(\nabla J_i) + [\dot{A}_i]_{\mathrm{chem}} = (\partial/\partial t)\,[A_i]\,. \qquad \text{(C.7)}$$

The energy conservation law may be formulated analogously and reads

$$\sum_{i=1}^{A}\left[-\int_{\partial G}(J_i E_i, \mathrm{d}f) - \int_{\partial G}(\tfrac{1}{2}M_i u_i^2 J_i, \mathrm{d}f) + \int_G E_i[\dot{A}_i]_{\mathrm{chem}}\,\mathrm{d}\tau\right] = \frac{\mathrm{d}}{\mathrm{d}t}\sum_{i=1}^{A}\left[\int_G E_i[A_i]\,\mathrm{d}\tau + \int_G \tfrac{1}{2}M_i u_i^2\,[A_i]\,\mathrm{d}\tau\right], \qquad \text{(C.8)}$$

with its associated differential equation

$$\sum_{i=1}^{A}\{-(\nabla, E_i J_i) - \tfrac{1}{2}M_i(\nabla, u_i^2 J_i) + E_i[\dot{A}_i]_{\mathrm{chem}}\} = \frac{\partial}{\partial t}\sum_{i=1}^{A}(E_i + \tfrac{1}{2}M_i u_i^2)\,[A_i]\,. \qquad \text{(C.9)}$$

Note that the first two terms on the left-hand side of (C.8) correspond to the transport of internal and kinetic energy across the boundary ∂G, whereas the third term corresponds to the chemically induced change in internal energy within G.

The general particle conservation equation (C.7) will now be applied to the example of the interconversion reactions in a molecular system with "trans" and "gauche" conformers (viz. 1,2-difluoroethane). Application to other conformers is straightforward. In the following the trans conformer will be denoted by A_t, whereas the two optical antipodes of the gauche conformation will be denoted by A_{g+} and A_{g-}. The symbols M and A will be used for the inert carrier gas and the A molecule in either one of its conformations, respectively.

The following elementary processes are assumed to be relevant (note that in each case the reverse process has to be considered as well):

$$\begin{aligned}
&\text{"type 1"} && -A_t - M + A_{g+} + M = 0\,,\\
&&& -A_t - M + A_{g-} + M = 0\,,\\
&&& -A_{g-} - M + A_{g+} + M = 0\,;\\
&\text{"type 2"} && -A_t - A + A_{g+} + A = 0\,,\\
&&& -A_t - A + A_{g-} + A = 0\,,\\
&&& -A_{g-} - A + A_{g+} + A = 0\,,\\
&\text{"type 3"} && -A_t + A_{g+} = 0\,,\\
&&& -A_t + A_{g-} = 0\,,\\
&&& -A_{g-} + A_{g+} = 0\,. \qquad \text{(C.10)}
\end{aligned}$$

The associated rate constants will be denoted by specifying initial and final conformation, e.g. $k_1(\mathrm{t}, \mathrm{g}+)$ and $k_1(\mathrm{g}+, \mathrm{t})$ for the forward and backward process of the first reaction in (C.10).

Owing to the fact that the optical antipodes of the gauche conformation are indiscernible in our experiments, we can substitute

$$[A_{g+}] = [A_{g-}] = \tfrac{1}{2}[A_g]\,. \qquad \text{(C.11)}$$

Moreover, by symmetry arguments the set of rate constants can be reduced to the following:

$$\begin{aligned}
&k_j(\mathrm{t}, \mathrm{g}+) = k_j(\mathrm{t}, \mathrm{g}-) = \tfrac{1}{2}k_j(\mathrm{t}, \mathrm{g})\,,\\
&k_j(\mathrm{g}+, \mathrm{t}) = k_j(\mathrm{g}-, \mathrm{t}) = \tfrac{1}{2}k_j(\mathrm{g}, \mathrm{t})\,,\\
&k_j(\mathrm{g}+, \mathrm{g}-) = k_j(\mathrm{g}-, \mathrm{g}+) = k_j(\mathrm{g}, \mathrm{g})\ \ (j = 1, 2, 3). \qquad \text{(C.12)}
\end{aligned}$$

Hence the rate equations read:

$$\begin{aligned}
[\dot{A}_t]_{\mathrm{chem}} &= -\{k_1(\mathrm{t},\mathrm{g})\,[M] + k_2(\mathrm{t},\mathrm{g})\,[A] + k_3(\mathrm{t},\mathrm{g})\}\,[A_t]\\
&\quad + \tfrac{1}{2}\{k_1(\mathrm{g},\mathrm{t})\,[M] + k_2(\mathrm{g},\mathrm{t})\,[A] + k_3(\mathrm{g},\mathrm{t})\}\,[A_g]\,, \qquad \text{(C.13)}
\end{aligned}$$

and

$$\begin{aligned}
[\dot{A}_g]_{\mathrm{chem}} &= -\tfrac{1}{2}\{k_1(\mathrm{g},\mathrm{t})\,[M] + k_2(\mathrm{g},\mathrm{t})\,[A] + k_3(\mathrm{g},\mathrm{t})\}\,[A_g]\\
&\quad + \{k_1(\mathrm{t},\mathrm{g})\,[M] + k_2(\mathrm{t},\mathrm{g})\,[A] + k_3(\mathrm{t},\mathrm{g})\}\,[A_t]\,. \qquad \text{(C.14)}
\end{aligned}$$

Note that the contributions of $k_j(\mathrm{g}, \mathrm{g})$ have cancelled out.

Before formulating the explicit particle conserva-

tion laws, the current density J_i of species A_i will be decomposed into a convective and a diffusive term (D_i = diffusion coefficient):

$$J_i = u_i[A_i] - D_i \nabla[A_i] . \qquad (C.15)$$

Moreover, in order to arrive at manageable expressions, a common diffusion coefficient D and a common flow velocity u will be assumed for all species. It should be noted, however, that velocity slip is not always negligible in supersonic molecular beams.

With these simplifications, the particle conservation for A_t and A_g reads:

$$\partial[A_i]/\partial t = -[A_i](\nabla, u) - (u, \nabla[A_i])$$
$$+ (\nabla, D\nabla[A_i]) + [\dot{A}_i]_{chem} \quad (i = t \text{ or } g) , \qquad (C.16)$$

with the reaction rates $[\dot{A}_i]_{chem}$ given by eqs. (C.13) and (C.14). For the carrier gas, eq. (C.16) is written without reaction rate term. In the case of stationary flow fields the left-hand side of (C.16) vanishes.

From these general conservation laws for a three-particle system subject to elementary chemical processes (C.10) and symmetries (C.11) and (C.12) the equations used in section 4 can be recovered. Introducing, as is customary in molecular-beam work, particle densities n_i and neglecting diffusion terms, one arrives at eq. (10) of the text. In the model calculations of section 4, unimolecular processes were found to be negligible (see also ref. [28]); by denoting rate constants as

$$k_{+j} = \tfrac{1}{2} k_j(g, t) , \qquad (C.17)$$

$$k_{-j} = k_j(t, g) , \qquad (C.18)$$

one finds the equivalent of eq. (17) in the text.

The energy conservation law will not be formulated explicitly in this paper since it leads to a very complicated set of coupled partial-differential equations. This omission is commented upon in (iv), section 5.

References

[1] J.B. Anderson, in: Molecular beams and low density gas dynamics, Vol. 4, ed. P.P. Wegener (Dekker, New York, 1974).

[2] D.H. Levy, L. Wharton and R.E. Smalley, in: Chemical and biochemical applications of lasers, Vol. 2, ed. C.B. Moore (Academic Press, New York, 1977).

[3] G.M. McClelland, K.L. Saenger, J.J. Valentini and D.R. Herschbach, J. Phys. Chem. 83 (1979) 947.

[4] P. Felder and Hs.H. Günthard, Chem. Phys. Letters 66 (1979) 283.

[5] J.B. Hopkins, D.E. Powers and R.E. Smalley, J. Chem. Phys. 72 (1980) 5039.

[6] P. Huber-Wälchli and Hs.H. Günthard, Chem. Phys. Letters 30 (1975) 347.

[7] P. Huber-Wälchli and Hs.H. Günthard, Spectrochim. Acta 37A (1981) 285.

[8] P. Felder and Hs.H. Günthard, Spectrochim. Acta 36A (1980) 223.

[9] P. Felder, T.K. Ha, A.M. Dwivedi and Hs.H. Günthard, Spectrochim. Acta 37A (1981) 337.

[10] P. Huber-Wälchli, Ph.D. Thesis No. 6339, ETH Zurich (1979).

[11] P. Felder and Hs.H. Günthard, J. Mol. Struct. 60 (1980) 297.

[12] A.H. Blatt, ed., Organic synthesis (Wiley, New York, 1963) p. 363.

[13] H.G. Bennewitz and B. Buess, Chem. Phys. 28 (1978) 175.

[14] R.J. Gallagher and J.B. Fenn, J. Chem. Phys. 60 (1974) 3487.

[15] D.R. Miller and R.P. Andres, J. Chem. Phys. 46 (1967) 3418.

[16] C.G.M. Quah, Chem. Phys. Letters 63 (1979) 141.

[17] C.G.M. Quah, J.B. Fenn and D.R. Miller, Proceedings of the 11th International Symposium on Rarefied Gas Dynamics (Commisariat à l'Energie Atomique, Paris, 1979) p. 885.

[18] C.E. Klots, J. Chem. Phys. 72 (1980) 192.

[19] J.D. Anderson, AIAA J. 8 (1970) 545.

[20] E.L. Knuth, in: Transportation engine emissions, eds. G.S. Springer and D. Patterson (Plenum Press, New York, 1972).

[21] E.L. Knuth, J. Chem. Phys. 66 (1977) 3515.

[22] P.K. Sharma, W.S. Young, W.E. Rodgers and E.L. Knuth, J. Chem. Phys. 62 (1975) 341.

[23] K. Bergmann, U. Hefter and P. Hering, Chem. Phys. 32 (1978) 329.

[24] E. Fehlberg, NASA Technical Report R-287 (1968).

[25] S. Mizushima, T. Shimanouchi, I. Harada, Y. Abe and H. Takeuchi, Can. J. Phys. 53 (1975) 2085.

[26] A.A. Frost and R.G. Pearson, Kinetics and mechanism (Wiley, New York, 1961).

[27] H. Ashkenas and F.S. Sherman, Rarefied Gas Dynamics, 4th Symposium, Vol. 2, ed. J.H. de Leeuw (Academic Press, New York, 1966) p. 84.

[28] P. Felder, Ph.D. Thesis No. 6789, ETH Zurich (1981).